Fuel xxx (2011) xxx–xxx

Contents lists available at ScienceDirect

Fuel

journal homepage: www.elsevier.com/locate/fuel

Accessibility of pores in coal to methane and carbon dioxide

Yuri B. Melnichenko [a,b,*], Lilin He [a], Richard Sakurovs [c,*], Arkady L. Kholodenko [d], Tomasz Blach [e], Maria Mastalerz [f], Andrzej P. Radliński [e,f], Gang Cheng [g,h], David F.R. Mildner [i]

[a] Neutron Scattering Sciences Division, Oak Ridge National Laboratory, Oak Ridge, TN 37831, USA
[b] Department of Physics and Astronomy, University of Tennessee, Knoxville, TN 37996, USA
[c] CSIRO Energy Technology, 11 Julius Avenue, North Ryde, 2113 NSW, Australia
[d] 375 H.L. Hunter Laboratories, Clemson University, Clemson, SC 29634-0973, USA
[e] Nanoscale Science and Technology Centre, Griffith University, Nathan 4111, Brisbane, Australia
[f] Indiana Geological Survey, Indiana University, Bloomington, IN 47405-2208, USA
[g] Sandia National Laboratories, Livermore, CA 94551, USA
[h] Sandia National Laboratories, Albuquerque, NM 87185, USA
[i] Center for Neutron Research, National Institute of Standards and Technology, Gaithersburg, MD 20899, USA

ARTICLE INFO

Article history:
Received 4 November 2010
Received in revised form 23 June 2011
Accepted 27 June 2011
Available online xxxx

Keywords:
Coal
Accessible pores
CO_2
Methane
Small-angle neutron scattering

ABSTRACT

Fluid–solid interactions in natural and engineered porous solids underlie a variety of technological processes, including geological storage of anthropogenic greenhouse gases, enhanced coal bed methane recovery, membrane separation, and heterogeneous catalysis. The size, distribution and interconnectivity of pores, the chemical and physical properties of the solid and fluid phases collectively dictate how fluid molecules migrate into and through the micro- and meso-porous media, adsorb and ultimately react with the solid surfaces. Due to the high penetration power and relatively short wavelength of neutrons, small-angle neutron scattering (SANS) as well as ultra small-angle scattering (USANS) techniques are ideally suited for assessing the phase behavior of confined fluids under pressure as well as for evaluating the total porosity in engineered and natural porous systems including coal. Here we demonstrate that SANS and USANS can be also used for determining the fraction of the pore volume that is actually accessible to fluids as a function of pore sizes and study the fraction of inaccessible pores as a function of pore size in three coals from the Illinois Basin (USA) and Bowen Basin (Australia). Experiments were performed at CO_2 and methane pressures up to 780 bar, including pressures corresponding to zero average contrast condition (ZAC), which is the pressure where no scattering from the accessible pores occurs. Scattering curves at the ZAC were compared with the scattering from same coals under vacuum and analysed using a newly developed approach that shows that the volume fraction of accessible pores in these coals varies between ~90% in the macropore region to ~30% in the mesopore region and the variation is distinctive for each of the examined coals. The developed methodology may be also applied for assessing the volume of accessible pores in other natural underground formations of interest for CO_2 sequestration, such as saline aquifers as well as for estimating closed porosity in engineered porous solids of technological importance.

1. Introduction

Fluids containing inorganic and organic solutes (including hydrocarbons) and gaseous species (e.g. carbon dioxide, CO_2, and methane, CH_4) can occupy the pores or fractures of numerous types of complex heterogeneous solids. These solid materials include such practical systems as supported catalysts, ceramics and composites, membranes, rock, minerals, soil, and bone. A number of factors dictate how fluids migrate into and through these micro- and meso-porous media, wet and ultimately adsorb and react with the solid surfaces. These include the size, shape, distribution and interconnectivity of pores, as well as the chemistry and physical properties of the solids and fluid molecules.

Coal is a porous material with pore sizes that span wide length scales including macro-, meso- and micro-porous regimes [1,2]. The porosity plays a key role in all aspects of coal utilization, such as extraction of methane from coal seams, gasification, combustions, liquefaction, production of metallurgical coke and activated carbon as well as geological sequestration of CO_2. The debate about the nature and structure of the pores in coal is ongoing [3,4]. According to a widely accepted consensus, coal is a solid that contains slit-like pores interconnected by narrow capillary

* Corresponding authors. Address: Neutron Scattering Sciences Division, Oak Ridge National Laboratory, Oak Ridge, TN 37831, USA. Tel.: +1 865 576 7746 (Y.B. Melnichenko), +61 02 94905309 (R. Sakurovs).
E-mail addresses: melnichenkoy@ornl.gov (Y.B. Melnichenko), Richard.Sakurovs@csiro.au (R. Sakurovs).

0016-2361/$ - see front matter © 2011 Published by Elsevier Ltd.
doi:10.1016/j.fuel.2011.06.026

constrictions and connected to the surface [5]. However, recent studies have suggested that a significant proportion of pores in coal may not be open to the external surface [6,7]. It is not known if pores in coal are inaccessible to green house gases such as methane and carbon dioxide, and the issue of selectivity of access to pores of different sizes is even more obscure. However, such information is particularly important for the practice of ECBM (enhanced coal bed methane recovery), a technique that uses injected CO_2 to increase the extraction efficiency of methane from coal seams. Experimental data on pore accessibility and adsorption selectivity could help to understand the fundamental limits to the ability of CO_2 to displace methane in subsurface conditions during sequestration of CO_2 in coal seams.

Here, we present a new approach for the experimental determination of the pore volume that is actually accessible to fluids as a function of pore size. The approach is based on the analysis of small-angle neutron scattering (SANS) patterns obtained from indigenous porous media and same media saturated with a contrast matching gas or supercritical fluid. We demonstrate the utility of the approach by determining the fraction of meso- and macro-pores that are accessible to methane and CO_2 as a function of pore size in several coals.

A number of experimental methods have been used to characterize porosity in solids, including gas adsorption [8], mercury intrusion porosimetry [10], transmission electron microscopy (TEM) [11], as well as small-angle scattering techniques (both small-angle neutron scattering, SANS [11] and small-angle X-ray scattering, SAXS [12]). Each of the methods has its limitations, e.g. gas adsorption and mercury porosimetry can only provide information about "open" porosity and TEM can only be used to assess pore connectivity inside a very limited sample volume. Thus far, SANS and SAXS in combination with corresponding ultra small-angle scattering techniques (USANS and USAXS) are non-invasive techniques that have been used for evaluating the total porosity (i.e. sum of the inaccessible and accessible pore volumes) over the range of pore sizes 0.4 nm–5 μm. The physical property probed by a neutron beam is called scattering length density (SLD). The scattering occurs on the interface between regions of different SLD values, which can be quantified *a priori* if both the mass density and chemical composition of each region are known. In great majority of coals there are two dominant regions of different SLD values: the solid coal matrix (with possibly slightly fluctuating SLD values) and the pore space. With proper mathematical processing of scattering data it is possible to determine the total porosity and surface area, pore size distribution, and other structural parameters [13,14].

In order to quantify the volume fraction of inaccessible pores, the porous solid may be saturated with "contrast matching" fluid, i.e. fluid with the SLD value close to that of the solid matrix. In this case, the scattering from open pores is eliminated and the residual scattering provides a "fingerprint" of the inaccessible porosity. SANS has been used before to evaluate the fraction of inaccessible pores in coal using *liquid mixtures* of protonated and deuterated solvents as a contrast matching medium. Gethner [15] employed

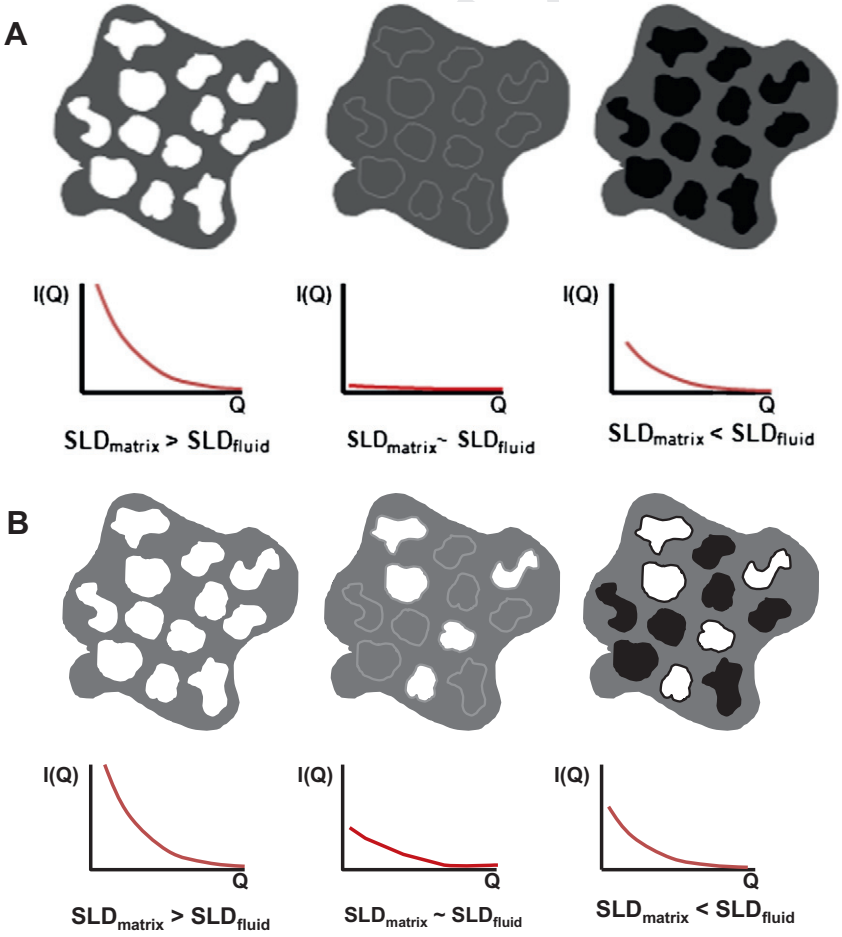

Fig. 1. Qualitative presentation of contrast-matching experiments with fluid saturated porous systems. (A) All pores are accessible to fluid molecules; (B) Pores are partially accessible to fluid molecules. In the latter case, the residual scattering at the zero average contrast condition can be used to quantify the volume fraction of accessible pores as a function of pore sizes, as explained in the text.

Please cite this article in press as: Melnichenko YB et al. Accessibility of pores in coal to methane and carbon dioxide. Fuel (2011), doi:10.1016/j.fuel.2011.06.026

mixtures of H_2O and D_2O to create contrast matching in coals. Based on the acquired SANS data, he concluded that all pores in the coal studied were completely filled by aqueous solutions and attributed residual scattering from the contrast matched coal to inhomogeneities in the organic matrix. These conclusions were later re-examined by Hall et al. [16–18] who also used H_2O/D_2O mixtures to eliminate scattering from open pores and concluded that some inaccessible pores existed in their coal samples. We note that in coals many of the functional groups can exchange hydrogen with water on time scales varying from seconds to weeks. Therefore, the isotope exchange may alter the H_2O/D_2O ratio in pores and significantly shift the local contrast matching condition, which was not fully recognized in previous studies [15–18].

An alternative method of obtaining contrast matching in porous media is to use non-adsorbing or weakly adsorbing supercritical fluids or gases, such as CO_2 or deuterated methane (d-methane) and measure the scattering patterns as a function of pressure. Using d-methane (CD_4) rather than "normal" methane (CH_4) helps to minimize the contribution of incoherent scattering from hydrogen to the SANS data. Furthermore, the SLD for methane can be varied with pressure and, unlike CH_4, d-methane has a positive SLD. An important advantage of utilizing gases or supercritical fluids is their excellent penetrability into porous structure due to their order(s) of magnitude lower viscosity than their corresponding liquids.

For a two-phase system with randomly distributed interconnected pores (e.g. coal with pores filled with air or weakly adsorbing fluid), the SANS intensity $I(Q)$ (neutron cross section per unit volume in units of cm^{-1}) is given by:

$$I(Q) = 4\pi(\rho_s^* - \rho_f^*)^2 c(1-C)V \int_o^\infty r^2 \gamma_0(r) \frac{\sin(Qr)}{Qr} dr, \quad (1)$$

where γ_0 is the normalized correlation function of the SLD fluctuations [11], $(\rho_s^* - \rho_f^*)^2 \equiv k_n^2$ is the neutron contrast between the SLD of the solid matrix (ρ_s^*) and the SLD of fluid in pores ($\rho_f^*; c = V_{pore}/V_{sample}$) is volume fraction of pores in the sample (total porosity), V is the volume of sample illuminated by the neutron beam, and $Q = 4\pi\lambda^{-1}\sin\theta$, in which 2θ is the scattering angle. In Eq. (1), ρ_f^* is proportional to the fluid density, which depends on pressure (P) and temperature (T). At small pressure $\rho_s^* \gg \rho_f^*$, and therefore neutron contrast and the intensity $I(Q)$ initially decreases with increasing P. If all pores are accessible to the fluid, $I(Q)$ should virtually vanish at a certain P, corresponding to the zero average contrast (ZAC) pressure (P_{ZAC}) at which $\rho_s^* = \rho_f^*$ and thus $k_N^2 = 0$. At $P > P_{ZAC}$, as ρ_f^* becomes greater than ρ_s^*, the scattering intensity $I(Q)$ will start increasing. In the two-phase approximation, any residual scattering observed at $P = P_{ZAC}$ is attributed to the scattering from inaccessible pores, which do not belong to the interconnected porous channels having access to the external surface (Fig. 1).

2. Materials and methods

2.1. Coals and porous silica

Three coal samples were investigated in this study: one from the Illinois Basin in the USA, collected from 167 m depth (Seelyville). Two other coals were samples of commercial coals from the Bowen Basin, Queensland, Australia. The selected coal samples have different total porosities and thus potentially different volume of accessible pores. In addition, they contain different proportions of the macerals; vitrinite is a dominant fraction in Seelyville and Coal 2, and inertinite is a dominant fraction in Coal 1. All coals were prepared in the form of coarse powder (particle size 1–0.5 mm), and all characterization was performed on this fraction (Table 1).

Porous fractal silica (PFS) samples were prepared by a template method, which was described in detail in [19]. The structure of thus obtained blank PFS samples with $\phi_s = 0.15$ was carefully characterized prior to these experiments [20,21]. Major structural parameters of the studied PFS include: cross-sectional fractal dimension $D_{cs} = 1.89$ and mass fractal dimension $D_m = 2.73$ (both corresponding to the pore size range 50 nm–30 μm), pore volume 1.24 cm^3/g, as well as specific area of 490 m^2/g. Pore size distribution of the studied PFS samples may be found in Figs. 9 and 13 in [22]. The volume fraction of silica $\phi_s = 0.15$ of the studied PFS, which corresponds to the porosity $P = 85\%$ was evaluated by weighing the solid and porous glass samples. Structural SANS study of CO_2 saturated sample at high pressure has shown that this porous silica is characterized by completely open porosity over the range of pore sizes between ~5 μm and ~40 Å [21].

The scattering length densities (SLDs) of the studied coals used for evaluating zero average contrast pressure P_{ZAC} were calculated as described in [13] based on their content of carbon and hydrogen (see Table 1). The SLD of porous silica was calculated using density of amorphous silica $\rho_{SiO_2} = 1.8$ g/cm^3. The results are listed in Table 2, which also shows the pressure and density of CD_4 at $T = 23$ °C and CO_2 at $T = 60$ °C at which the SLD of each porous matrix is contrast matched by the fluid. As was shown in [21,23], SLDs of CO_2 and CD_4 at any particular fluid density, temperature and pressure may be calculated using the following equations:

$$\rho^*_{CO_2} = [2.49 \cdot (\rho_{CO_2})_{bulk}]10^{10}\ cm^{-2}$$

$$\rho^*_{CD4} = [10 \cdot (\rho_{CD4})_{bulk}]10^{10}\ cm^{-2}$$

where ρ^* is the fluid SLD. All fluid density calculations were performed using equations of state from in the REFPROP software available from National Institute of Standards and Technology [24]. Densities of deuterated methane CD_4 were calculated from densities of normal methane by multiplying ρ_{CH_4} by a factor 1.25 (the ratio of atomic weights of deuterated and protonated methane).

2.2. SANS and USANS experiments

SANS experiments were conducted at ORNL on the General Purpose SANS instrument [25] with neutron wavelengths of $\lambda = 12$ Å and $\lambda = 4.8$ Å ($\Delta\lambda/\lambda \sim 0.13$). Sample-detector distances were chosen

Table 2
Scattering length densities of coal and silica xerogel.

Sample	SLD (10^{10} cm^{-2})	P_{ZAC} (bar)/ρ_{CD4} (g/cm^3, 23 °C)	P_{ZAC} (bar)/ρ_{CO_2} (g/cm^3, 60 °C)
Seelyville	2.20	224.7/0.220	380.1/0.88
Coal 1	3.45	504.7/0.345	–
Coal 2	2.34	246.7/0.234	–
Porous silica	3.47	514.3/0.347	–

Table 1
Selected characteristics of coal samples.

Coal	Hg porosity (%)	Ash (% db)	C (% daf)	H (% daf)	He Dens (g/mL)	$R_{v,max}$ (%)	Vitrinite (vol.% mmf)	Liptinite/inertinite (vol.% mmf)/(vol.% mfm)
Seelyville	8.3	8.02	79.36	5.82	1.49	0.53	91.3	4.8/3.9
Coal 1	16.1	20.3	80.7	3.9	1.594	0.62	23.9	1.6/74.5
Coal 2	7.0	5.6	84.1	5.7	1.313	0.95	82.6	4.1/13.3

Please cite this article in press as: Melnichenko YB et al. Accessibility of pores in coal to methane and carbon dioxide. Fuel (2011), doi:10.1016/j.fuel.2011.06.026

to cover an overall range of scattering vectors (Q) $0.0016 < Q < 0.2$ Å^{-1}, where $Q = 4\pi\lambda^{-1}\sin\theta$, in which 2θ is the scattering angle. The data were corrected for instrumental background as well as detector efficiency and put on absolute scale [cross section $I(Q)$ in units of cm^{-1}] by means of pre-calibrated secondary standards. USANS experiments were performed at NIST, using the BT5 perfect crystal SANS instrument ($\lambda = 2.4$ Å, Q-range $5 \times 10^{-5} < Q < 0.003$ Å^{-1} [26]. Application of these instruments allowed a broad range of pore sizes, from approximately 10,000 Å to 12 Å to be probed by neutrons. The characteristic pore size may be estimated based on the Bragg law $\lambda = 2D\sin\theta$, where for disordered systems D is the characteristic length scale of the structural inhomogeneities (e.g. linear pore size in a coal matrix). This law provides an approximate relationship between the scattering vector Q and R: $R \approx 2\pi/Q$. Detailed simulations show that for polydisperse porous media a more appropriate relationship is $R \approx 2.5/Q$ [13], which was used in this work to relate Q-values with R.

For both SANS and USANS experiments, coal or silica powders were confined inside a thin-wall aluminium container with internal thickness of 1 mm. Samples were dried overnight under vacuum at 60 °C and subsequently mounted inside the ORNL high-pressure cell that has been used extensively for previous neutron scattering experiments with CO_2-saturated coals as well as engineered porous materials [21,23,27–31]. The neutron beam size used was about 3 cm^2 in area and acquisition times were of the order of 30 min for SANS and several hours for USANS. SANS and USANS scattering profiles of CD_4 saturated samples were acquired at room temperature $T = 23$ °C in the pressure range from 0 to ~640 bar of CD_4 (Air Liquide, 99% purity). SANS and USANS profiles of Seelyville coal with supercritical CO_2 (Air Liquide, SFC purity 99.99%) were obtained at temperature 60 °C in the pressure range 0 to ~550 bar. In this experiment the sample temperature was controlled with a precision of ±0.1 °C using electric heaters and a precision temperature controller. The pressure was increased stepwise using a custom-built pressure intensifier and measured using a precision pressure transducer. All measurements were started ~10 min after fluid injection to allow for equilibrium saturation of the pores with CD_4 or CO_2 at each pressure.

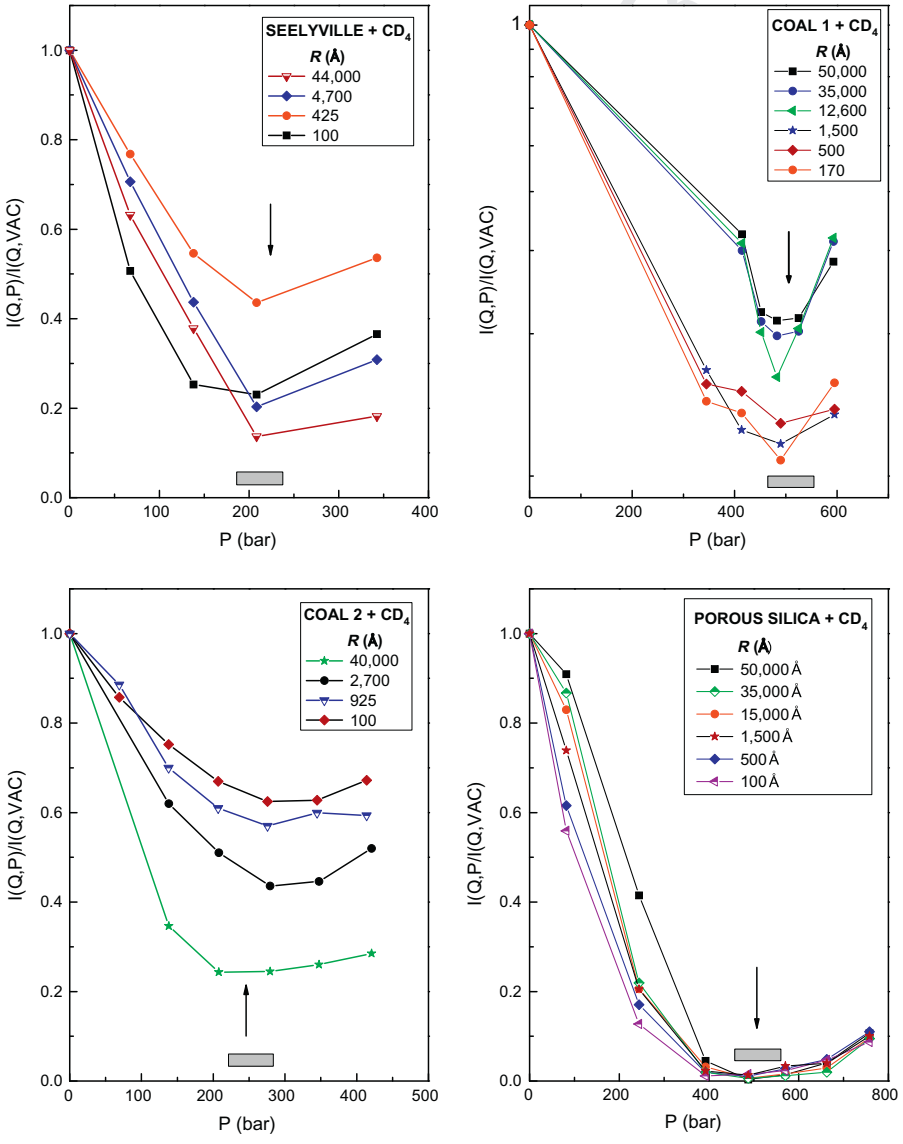

Fig. 2. The variation of the normalized scattering as a function of pressure of d-methane for coals and porous silica in pores of different sizes R (see insets). The arrows show calculated pressures at which zero average contrast condition is reached for each combination of the porous matrix and fluid. Grey boxes indicate the experimental estimate of deviation from the calculated value of P_{ZAC}, (±10% for Seelyville and Coal 2, and ±5% for Coal 1 and porous silica).

Please cite this article in press as: Melnichenko YB et al. Accessibility of pores in coal to methane and carbon dioxide. Fuel (2011), doi:10.1016/j.fuel.2011.06.026

3. Results and discussion

In compositionally complex porous matrices, such as coal, the scattering from "dry" samples may contain a small contribution that originates from fluctuations of the SLD due to the presence of chemical inhomogeneity of the organic matter and/or various inclusions, such as mineral matter. Careful analysis has shown that this contribution usually does not exceed 5–10% of the total scattering [14,16]. However it may become accentuated near ZAC due to the suppression of scattering from open pores of all sizes. To examine this issue, we observe that the zero average contrast condition for all porous solids studied here is actually achieved at P_{ZAC} values that have been calculated from the equations of state for corresponding bulk fluids and the chemical composition of each matrix. In Fig. 2 we show the ratio of the scattering intensity measured at several pressure values, $I(Q, P)$, to the intensity measured under vacuum $I(Q, \mathrm{VAC})$, corresponding to pores of different sizes in four different samples (three coals and a man-made porous silica). Detailed simulations show that for polydisperse porous media such as coal more than half of the scattering intensity measured at a scattering vector Q_i is contributed by pores whose linear dimension, R_i, lies in a narrow range around the mean value of $R_i \approx 2.5/Q_i$ [13]. It transpires that for each sample the minimum scattering intensity is reached close to the calculated value of P_{ZAC}. Furthermore, the scattering intensity shows only minor variation with pressure around P_{ZAC} and the deviation of the pressure corresponding to the scattering minimum from P_{ZAC} in pores of different sizes does not exceed ~10% for Seelyville and Coal 2, and ~5% for Coal 1 and porous silica. The observed agreement between the calculated and measured values of P_{ZAC} indicates a close proximity of the densities of the adsorbed and unadsorbed fluid phases at high pressures in pores of sizes varying from ~100 Å to 2.5 μm. Very importantly, curves presented in Fig. 2 show a monotonic decrease as the pressure approaches the calculated P_{ZAC} value followed by a monotonic increase. This indicates that a possible contribution of inhomogeneities with SLD (and, consequently, P_{ZAC}) different from the matrix is not significant across the entire range of pore sizes, with the notable exception of the small pores (⩽100 Å), for which condensation effects have modified the shape of scattering curves. Such condensation effects have been subject of recent SANS studies of the phase behavior of gases and supercritical fluids in micropores of natural and engineered porous materials [21,23,27,28].

Fig. 3 shows the combined USANS and SANS patterns from the coals and porous silica, measured in vacuum and at $P \approx P_{ZAC}$. The relatively strong residual scattering from contrast-matched coals indicates the presence of significant number of pores, accessible to neither supercritical CO_2 nor methane. The scattering patterns at $P = P_{ZAC}$ show distinctive deviations from $I(Q)$ in vacuum that vary with each sample. Whereas all samples reveal a substantial decrease in $I(Q)$ in the low-Q range (indicating that most of the large pores are accessible to the fluid), the reduction of intensity in the intermediate Q-range is less accentuated and is Q-dependent. For Coal 1, the curve $I(Q, P_{ZAC})$ is virtually parallel to $I(Q)$ acquired in vacuum. The strongest decline in scattering at P_{ZAC} is observed for porous silica: it exceeds five orders of magnitude at the limit of low Q, and about two orders of magnitude for larger values of the scattering vector.

We demonstrate in Appendix A that the ratio of $I(Q_i, P_{ZAC})$ and $I(Q_i, \mathrm{VAC})$ may be used to calculate the volume fraction of *accessible pores* $c_{AC}(Q_i)$ *at any arbitrary value of the scattering vector* Q_i (or, equivalently, at any pore size, $R_i \approx 2.5/Q_i$):

$$\frac{I(Q_i, P_{ZAC})}{I(Q_i, \mathrm{VAC})} \cong 1 - C_{AC}(Q_i), \tag{2}$$

where $c_{AC}(Q_i)$ is defined as the ratio of the volume of accessible pores to the total pore volume at a given pore size. Consequently a negligible change in the scattering intensity measured at zero average contrast pressure $I(Q_i, P_{ZAC})$ relative to the intensity mea-

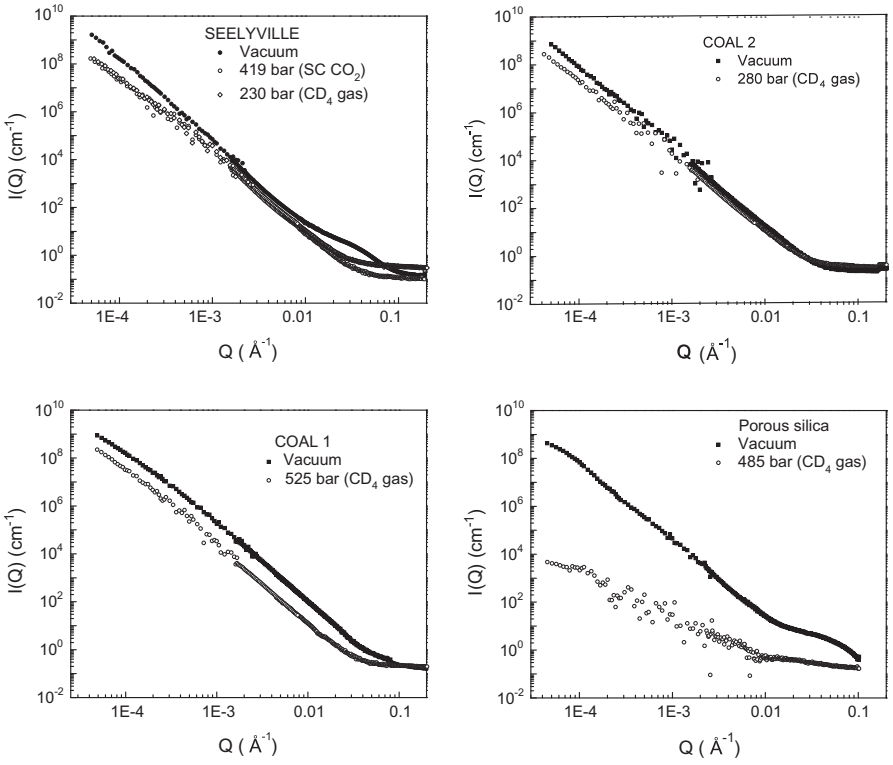

Fig. 3. Combined USANS and SANS curves acquired from coals and porous silica in vacuum and at zero average contrast pressures (as indicated in the insets).

Please cite this article in press as: Melnichenko YB et al. Accessibility of pores in coal to methane and carbon dioxide. Fuel (2011), doi:10.1016/j.fuel.2011.06.026

sured under vacuum $I(Q_i, \mathrm{VAC})$ in some region Q_i indicates a low accessibility of gases into pores of sizes $R_i \sim 2.5/Q_i$. Conversely, if gases can penetrate into pores of that size, a relatively large change in that ratio may be anticipated. Fig. 4 shows the variation of the volume fraction of accessible pores in the studied coals and porous silica as a function of Q_i and R_i calculated using Eq. (2). As may be seen in Fig. 4, for the test sample (porous silica) the values of $I(Q_i, P_{ZAC})$ are much smaller than $I(Q_i, \mathrm{VAC})$ for all values of Q_i so that the value of C_{AC} is approximately equal to unity for pores of all sizes. This result was expected based on our previous studies of the same porous silica sample, which demonstrated that its porous fractal structure is completely open to fluid molecules [21]. In contrast, the variation of $C_{AC}(R)$ for each coal sample is radically different from that for porous silica and also varies from coal to coal. For the Seelyville coal, macropores larger than $\sim$ 1000 Å are equally accessible to both CO_2 and d-methane molecules, and the value of C_{AC} for both fluids gradually decreases from $\sim$0.9 to $\sim$0.55. At the same time, pores inside the size range $1000 > R > 100$ Å appear to be more accessible to CO_2 molecules (by $\sim$10%). We tentatively attribute this subtle but measurable difference to a smaller size of CO_2 molecules, which makes it easier to penetrate narrow capillary constrictions joining the pores. For Coal 1, the ratio of $I(Q_i, \mathrm{VAC})$ to $I(Q_i, P_{ZAC})$ and thus c_{AC} is approximately constant over a large range of Q_i, and the volume fraction of accessible pores is generally much larger than for the other coals. About 80–85% of both macro- and meso-pores within the size range from 100 to 25,000 Å are accessible to d-methane. For Coal 2, the variation of C_{AC} with pore size is qualitatively similar to that of the Seelyville except of the upturn for pore sizes $R < 700$ Å. Error bars in Fig. 4 are based on the estimated fluctuations of the SLD in different pores in each sample (see discussion of Fig. 2). The possible modification of the distribution function $c_{AC}(R)$ by a small scattering contribution from inclusions and inhomogeneities near the contrast matching condition is estimated by error bars shown in Fig. 4.

4. Conclusions

In this paper, we demonstrated for the first time that SANS and USANS can be used for determining the fraction of the pore volume in porous media that is actually accessible to fluids as a function of pore sizes. The proposed new methodology was used to study volume of pores accessible to methane and CO_2 in three coals from the Illinois Basin (USA) and Bowen Basin (Australia). The proposed relation between scattering intensities and the volume fraction of accessible pores (Eq. (2)) in combination with relationship between real and inverse space dimensions was used to analyse the differences in scattering intensities measured at zero average contrast pressure and under vacuum (Fig. 3) and to calculate the variation of the volume fraction of accessible pores as a function of pore sizes in the studied coals (Fig. 4). The results presented in this article constitute evidence of the existence of closed pores in coal that are inaccessible to the molecules of supercritical CO_2 and d-methane on the time scale of performed experiments [32]. Each coal has its own "fingerprint" distribution of C_{AC} as a function of pore size in the meso- and macroporous regions. The fraction of pores accessible to CO_2 and methane appears to be relatively large in highly porous inertinite-rich Coal 1. It is much lower in vitrinite-rich, low-porosity Seelyville and Coal 2 coals, both of which demonstrate qualitatively similar but yet not identical variation of

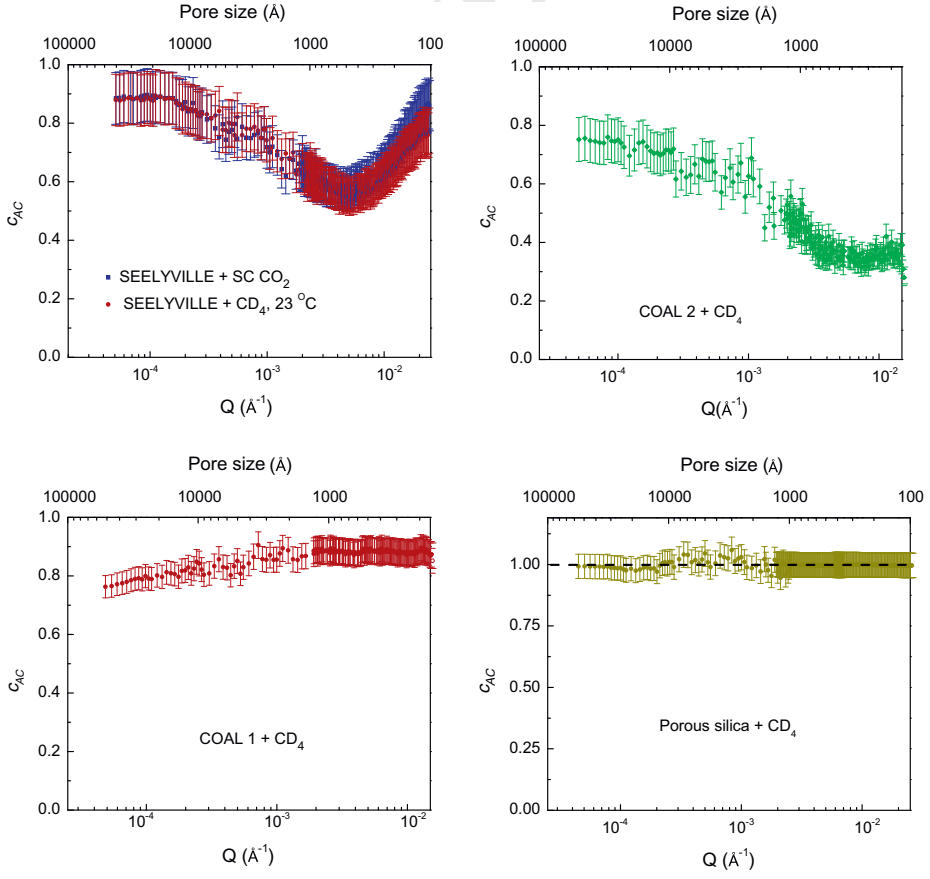

Fig. 4. The variation of the volume fraction of pores accessible to green house gases as a function of the scattering vector and pore size calculated for the samples of coal and porous silica. The error bars correspond to C_{AC} ±10% for Seelyville and Coal 2, and C_{AC} ±5% for Coal 1 and porous silica.

Please cite this article in press as: Melnichenko YB et al. Accessibility of pores in coal to methane and carbon dioxide. Fuel (2011), doi:10.1016/j.fuel.2011.06.026

$C_{AC}(R)$. Based on these observations we speculate that the amount of accessible pores in coal may be directly related to the total porosity as probability of the formation of the interconnected network of pores accessible to fluids should be facilitated in higher porosity coals. We believe that the observed coexistence of inaccessible and accessible pores may help to resolve the inconsistency between the existing models of the coal structure, one of which is based on the assumption of interconnectivity and thus total accessibility of pores [5] and the other advocates predominantly closed porosity [6]. Our data demonstrate that both types of pores may be present in coal samples. Finding reliable correlations between closed porosity and other major physical and chemical parameters of colas (total porosity, elemental and maceral composition, rank, etc.) will require systematic SANS/USANS studies of coal samples from different origin.

Finally, we note that pore accessibility and its variation with pore size are not defined solely by the structure of a specific porous solid. Accessibility may vary considerably depending on temperature and pressure, which determine the phase of the invading medium (i.e. gas, liquid, or supercritical fluid) as well as on the chemistry-driven specifics of the molecule–surface interaction potentials. Even for a particular solid/fluid combination, the accessible porosity and the variation of $C_{AC}(R)$ may depend on the proximity of the fluid phase state to its critical point at which the critical adsorption effects may become dominant [33]. In the case of coal and other organic porous materials, the measured $C_{AC}(R)$ may also depend on the time scale of the experiment, as the molecular diffusion in such solids might occur quickly through an interconnected network of pores having access to the external surface as well as slowly through the solid matrix. Establishing quantitative relationship between the microstructure and matrix chemistry of a porous solid and the accessibility of its pore space to an invading fluid in an arbitrary thermodynamic state is a complex task. The methodology described here may be used for *in situ* quantification of coal pores accessible to CO_2 and methane at temperatures and pressures corresponding to subsurface conditions. Such experiments may help to refine existing methods used for calculating saturation capacity of subsurface gas reservoirs as well as to improve models used for evaluating the kinetics of methane production from coal seams, thus providing essential information for ECBM technologies and geological storage of anthropogenic carbon. It may be also applied for assessing the volume of accessible pores in other natural underground formations of interest for CO_2 sequestration, such as saline aquifers as well as for estimating the fraction of pores that are inaccessible to fluids in engineered porous solids of technological importance.

5. Uncited reference

Q2 [9].

Acknowledgements

This research at Oak Ridge National Laboratory's High Flux Isotope Reactor was sponsored by the Laboratory Directed Research and Development Program and the Scientific User Facilities Division, Office of Basic Energy Sciences, US Department of Energy. This research was supported in part by the ORNL Postdoctoral Research Associates Program, administered jointly by the ORNL and the Oak Ridge Institute for Science and Education. The elements of this work utilizing the BT-5 instrument at the NCNR were supported in part by the National Science Foundation under agreement No. DMR-0454672. Mention of specific commercial products is for informational purposes only and does not constitute endorsement by the National Institute of Standards and Technology.

Appendix A. Derivation of the Eq. (2) in the main text

A.1. Porod invariant

Following Porod [12], we define the static scattering structure factor $S(\mathbf{Q})$ as

$$S(\mathbf{Q}) = \langle \Delta\rho(\mathbf{Q})\Delta\rho(-\mathbf{Q})\rangle = \langle |\Delta\rho(\mathbf{Q})|^2\rangle, \tag{A.1}$$

where $\langle\cdots\rangle$ denotes the equilibrium statistical mechanical average while $\Delta\rho(\mathbf{Q})$ denotes the Fourier transformed fluctuation density. The experimentally measured data for $S(\mathbf{Q})$ can be used for restoration of the density–density correlator $\check{S}(\mathbf{r})$ in coordinate space. Indeed, we obtain

$$\check{S}(\mathbf{r}) = \frac{1}{(2\pi)^3}\int d\mathbf{Q}\exp(i\mathbf{Q}\cdot\mathbf{r})S(\mathbf{Q}). \tag{A.2}$$

Up to a constant, the Porod invariant can now be defined as $\check{S}(\mathbf{r}=0)$. At the same time, it is well known from thermodynamics [34] that $S(\mathbf{Q}=0)$ can be obtained with help of the thermodynamic sum rule as usual. In Porod's notations (e.g. see page 28 in [12]) we write

$$S(\mathbf{Q}=0) = V^2\langle(\Delta\rho^2)\rangle, \tag{A.3}$$

where V is the volume of the sample. To determine the volume, Porod defines (without derivation) on the same page the invariant

$$\check{S}(\mathbf{r}=0) = 2\pi^2 V\langle(\Delta\rho^2)\rangle \tag{A.4}$$

now known in the literature as Porod invariant [34]. By combining Eqs. (A.3) and (A.4), the volume V can be determined. For the purposes of this work we would like to re-derive the Porod invariant and to explain why, indeed, it is an invariant. To do so, we derive the following chain of equalities

$$\begin{aligned}\check{S}(\mathbf{r}=0) &= \frac{1}{(2\pi)^3}\int d\mathbf{Q}S(\mathbf{Q}) = \frac{1}{(2\pi)^3}\int d\mathbf{Q}\langle\Delta\rho(\mathbf{Q})\Delta\rho(-\mathbf{Q})\rangle\\ &= \frac{1}{(2\pi)^3}\int d\mathbf{Q}\int d\mathbf{r}\int d\mathbf{r}'\exp[-i\mathbf{Q}\cdot(\mathbf{r}-\mathbf{r}')]\\ &\quad\times\langle\Delta\rho(\mathbf{r})\Delta\rho(\mathbf{r}')\rangle\\ &= \int d\mathbf{r}\langle(\Delta\rho(\mathbf{r}))^2\rangle = const V\langle(\Delta\rho(0))^2\rangle = 2\pi^2 V\langle\Delta\rho^2\rangle.\end{aligned} \tag{A.5}$$

The *const* was determined by the angular averaging, as usual. At the same time, the above can be also written as

$$\int d\mathbf{Q}S(\mathbf{Q}) = \int d\mathbf{Q}\langle\Delta\rho(\mathbf{Q})\Delta\rho(-\mathbf{Q})\rangle = (2\pi)^3\int d\mathbf{r}\langle(\Delta\rho(\mathbf{r}))^2\rangle \tag{A.6}$$

Eq. (A.6) can be recognized as Parseval's formula used in the theory of Fourier transforms. For our readers convenience we would like to reobtain this formula now.

A.2. Porod invariant and Parseval's formula

To begin, we would like to remind our readers the basic facts about this formula. For this purpose, let $f(\mathbf{r})$ be some arbitrary well behaved function whose Fourier transform is given by

$$F(\mathbf{r}) = \frac{1}{(2\pi)^3}\int d\mathbf{Q}\exp(i\mathbf{Q}\cdot\mathbf{r})\cdot f(\mathbf{r}). \tag{A.7}$$

Accordingly, its inverse transform is given by

$$f(\mathbf{Q}) = \int d\mathbf{r}\exp(-i\mathbf{Q}\cdot\mathbf{r})\cdot f(\mathbf{r}). \tag{A.8}$$

Using these definitions, consider the following chain of equalities

$$\int d\boldsymbol{r}(f(\boldsymbol{r}))^2 = \int d\boldsymbol{r} f(\boldsymbol{r}) \frac{1}{(2\pi)^3} \int d\boldsymbol{Q} exp(i\boldsymbol{Q}\cdot\boldsymbol{r}) f(\boldsymbol{Q})$$
$$= \frac{1}{(2\pi)^3} \int d\boldsymbol{Q} f(\boldsymbol{Q}) \int d\boldsymbol{r} f(\boldsymbol{r}) exp(i\boldsymbol{Q}\cdot\boldsymbol{r})$$
$$= \frac{1}{(2\pi)^3} \int d\boldsymbol{Q} f(\boldsymbol{Q}) f(-\boldsymbol{Q})$$
$$\equiv \frac{1}{(2\pi)^3} \int d\boldsymbol{Q} |f(\boldsymbol{Q})|^2. \quad \text{(A.9A)}$$

In this expression $|f(\boldsymbol{Q})|^2 = f(\boldsymbol{Q})f(-\boldsymbol{Q}) \equiv f(\boldsymbol{Q})f(\boldsymbol{Q})^*$, where $*$ denotes complex conjugation. The expression (S9A) is the Parseval identity. That is

$$\int d\boldsymbol{r}(f(\boldsymbol{r}))^2 = \frac{1}{(2\pi)^3} \int d\boldsymbol{Q} |f(\boldsymbol{Q})|^2. \quad \text{(A.9B)}$$

It is useful now to compare this result with Eq. (A.6). To do so, we have to make the following identifications

$$(2\pi)^3 \int d\boldsymbol{r}[f(\boldsymbol{r})]^2 \rightleftarrows (2\pi)^3 \int d\boldsymbol{r}\langle[\Delta\rho(\boldsymbol{r})]^2\rangle$$

and

$$\int d\boldsymbol{Q}|f(\boldsymbol{Q})|^2 \rightleftarrows \int d\boldsymbol{Q} S(\boldsymbol{Q})$$

Parseval's formula can be written in many different ways. For instance, instead of Eq. (A.8) we can write $f(\boldsymbol{r}) = \sum_i a_i\phi_i(\boldsymbol{r})$, where we assume that $\int |\phi_i(\boldsymbol{r})|^2 d\boldsymbol{r} = 1$ and $\int \varphi_i^*(\boldsymbol{r})\varphi_j(\boldsymbol{r})d\boldsymbol{r} = \delta_{ij}$. Using this result we obtain

$$\int d\boldsymbol{r}[f(\boldsymbol{r})]^2 = \sum_i |a_i|^2. \quad \text{(A.10)}$$

This result can be looked upon as follows. Replace integration by summation in Eq. (A.9B), that is write

$$\sum_i (\Delta\boldsymbol{r})^3 [f(\boldsymbol{r}_i)]^2 = \sum_i \frac{(\Delta\boldsymbol{Q})^3}{(2\pi)^3} |f(\boldsymbol{Q}_i)|^2. \quad \text{(A.11)}$$

By doing so, we effectively put our system onto some (say, cubic) lattice with effective size of the cell of order $\Delta\boldsymbol{r}$ in real space and $\Delta\boldsymbol{Q}$ in reciprocal space. By analogy with quantum mechanics, let now $\Delta\boldsymbol{r}\ \Delta\boldsymbol{Q} = \Theta$, where Θ is some constant. Such result makes sense in view of the wave nature of light (or neutrons). Such Heisenberg-type relation was used successfully already by Radlinski [13] in his computer simulations of neutron scattering from coals. In his work the constant Θ was estimated as 2.5. With account of such a relation, we can rewrite Eq. (A.11) as follows

$$\sum_i \langle[\Delta\rho(\boldsymbol{r}_i)]^2\rangle = \frac{(\Delta\boldsymbol{Q})^6}{(2\pi)^3} \frac{1}{\Theta^3} \sum_i S(\boldsymbol{Q}_i) \quad \text{(A.12)}$$

Equivalently, the above results are just the discretised form of Eq. (A.6). We shall use this form of Parseval's identity below.

A.3. Porod invariant to Eq. (2) of the main text

We would like now to generalize the obtained result, Eq. (A.12), by extending it to two-phase systems. For this purpose, in view of the fact that Eq. (A.12) is written for the cubic lattice, we can use known results from the scattering theory for solid alloys [35]. We begin by introducing random numbers c_i such that $c_i = 1$ (if the ith site is occupied by phase 1) and $c_i = 0$ (if the ith site is occupied by phase 2). The average $\langle C_i\rangle$ can now be defined as

$$\langle C_i\rangle = C = \frac{1}{N}\sum_i^N C_i,$$

where summation takes place over all lattice sites. Also, in view of definition of c_i it follows that $C_i^2 = C_i$. Consider now $\Delta\rho(\boldsymbol{r}_i)$ for such two phase system. In the case of just one phase we define fluctuation of density as $\Delta\rho(\boldsymbol{r}_i) = \rho(\boldsymbol{r}_i) - \rho$, where ρ is homogeneous reference density. In the case of two phases, we have $\rho \to c\rho_1 + (1-C)\rho_2$ and $\Delta\rho(\boldsymbol{r}_i) = C_i\rho_1 + (1-C_i)\rho_2 - [c\rho_1 + (1-c)\rho_2] = (C_i - c)\rho_1 - (C_i - c)\rho_2$.

Consider now the average

$$\langle\Delta\rho(\boldsymbol{r}_i)^2\rangle = \langle[(C_i - C)\rho_1]^2\rangle + \langle[(C_i - C)\rho_2]^2\rangle - 2\rho_1\rho_2\langle(C_i - C)^2\rangle$$
$$= (\rho_1 - \rho_2)^2\langle(C_i - C)^2\rangle = (\rho_1 - \rho_2)^2 C(1 - C)$$

Using this result we obtain,

$$\sum_i S(\boldsymbol{Q}_i) = 2\pi^2 V(\rho_1 - \rho_2)^2 c(1 - C), \quad \text{(A.13)}$$

where averaging over angles was made. Explicitly, we took into account that $\frac{(2\pi)^3}{4\pi} = 2\pi^2$ and that $(\Delta\boldsymbol{r})^3\sum_i = V$. Here and below we shall assume that $(\Delta\boldsymbol{r})^3$ is of order of Θ^3 so that $V = N\Theta^3$. The constant factor $(\Delta\boldsymbol{Q})^3$ was absorbed into definition of $S(\boldsymbol{Q})$ since it is not essential (see below). Thus, Eq. (A.13) is the standard result by Porod [12].

This result should now be looked upon as follows. Following book by Krivoglaz [35], especially taking into account his Eq. (1.15) on page 11, we can think not only about the averages of the type $\frac{1}{N}\sum_{i=1}^N (C_i - C)^2 = C(1-C)$ in the *direct* lattice but also about analogous averages in the *dual* lattice, which in the present case is cubic also. In such a case, we can use Eqs. (A.1), (A.11), (A.12) in order to write

$$S(\boldsymbol{Q}_i) = \langle|\Delta\rho(\boldsymbol{Q}_i)|^2\rangle \quad \text{(A.14)}$$

In order to perform averaging over random variables $\Delta\rho(\boldsymbol{Q}_i)$ we have to take into account that

$$\Delta\rho(\boldsymbol{Q}_i) = \frac{1}{V}\sum_j \Delta\rho(\boldsymbol{r}_j)\exp(i\boldsymbol{Q}_i\cdot\boldsymbol{r}_j) \quad \text{(A.15)}$$

and $V = N\Theta^3$ as before. To evaluate $\langle[\Delta\rho(Q_i)]^2\rangle$ using Eq. (A.15), following Ref. [35] (page 11, Eq. (1.15)), we introduce density-related variable $c(\boldsymbol{Q}_i)$ in such a way that

$$\frac{1}{N}\sum_{i=1}^n C(\boldsymbol{Q}_i)[(1 - C(\boldsymbol{Q}_i))] = C(1 - C) \quad \text{(A.16)}$$

In view of Eqs. (S12, 13) Q3

$$S(\boldsymbol{Q}_i) = \omega C(\boldsymbol{Q}_i)(1 - C(\boldsymbol{Q}_i)) \quad \text{(A.17)}$$

The constant ω is known in principle but unimportant since it will be subsequently eliminated. To get rid of this constant, we determine the ratios of the type

$$\frac{S(\boldsymbol{Q}_i, P_{ZAC})}{S(\boldsymbol{Q}_i, VAC)} = \frac{C_{IN}(\boldsymbol{Q}_i)[1 - C_{IN}(\boldsymbol{Q}_i)]}{C(\boldsymbol{Q}_i)[(1 - C_i(\boldsymbol{Q}_i))]}, \quad \text{(A.18)}$$

where $S(\boldsymbol{Q}_i, P_{ZAC})$ and $S(\boldsymbol{Q}_i, VAC)$ is the structure factor from fluid saturated coal at zero average contrast pressure P_{ZAC} and the structure factor of the coal under vacuum, respectively. Furthermore, $C(\boldsymbol{Q}_i)$ is the volume fraction of all pores (see Eq. (1) of the main text) and $c_{IN}(\boldsymbol{Q}_i)$ is the volume fraction of *inaccessible* pores defined as the ratio of the volume of *inaccessible pores* to the *total pore volume*. For low porosity samples such as coal both c and $c_{IN} \ll 1$, and for any arbitrary value of the scattering vector $\boldsymbol{Q}_i$ (or equivalently at corresponding pore size $R_i = 2.5/\boldsymbol{Q}_i$) we have

$$\frac{C_{IN}(\boldsymbol{Q}_i)(1 - C_{IN}(\boldsymbol{Q}_i))]}{c(\boldsymbol{Q}_i)(1 - c(\boldsymbol{Q}_i))} \cong \frac{c_{IN}(\boldsymbol{Q}_i)}{c(\boldsymbol{Q}_i)} = 1 - C_{AC}(\boldsymbol{Q}_i) \quad \text{(A.19)}$$

or

$$\frac{S(\mathbf{Q}_i, P_{ZAC})}{S(\mathbf{Q}_i, \mathrm{VAC})} \cong 1 - C_{AC}(\mathbf{Q}_i), \tag{A.20}$$

where c_{AC} ($\mathbf{Q}_i$) is the volume fraction of *accessible pores* at $\mathbf{Q}_i$ is defined as the ratio of the volume of *accessible pores to the total pore volume*. Eq. (A.20) is Eq. (2) of the main text. It can be used for evaluating the volume fraction of accessible pores as a function of $\mathbf{Q}_i$ (or $\mathbf{R}_i$) by measuring SANS/USANS patterns from the "dry" and contrast matched samples and finding the ratio of the scattering intensities at each $\mathbf{Q}_i$.

References

[1] Anderson RB, Hall WK, Lecky JA, Stein KC. Sorption studies on American coals. J Phys Chem 1956;60:1548–58.
[2] Gan H, Walker PL, Nandi SP. Nature of porosity in American coals. Fuel 1972;51:272–7.
[3] White CM, Smith DH, Jones KL, Goodman AL, Jikich SA, LaCount RB, et al. Sequestration of carbon dioxide in coal with enhanced coalbed methane recovery – a review. Energy Fuels 2005;19:659–724.
[4] Mahajan OP. CO_2 surface area of coals – the 25-year paradox. Carbon 1991;29:735–42.
[5] Bond RL. Capillary structure of coal. Nature 1956;178:104–5.
[6] Larsen JW, Wernett P. Pore structure of Illinois #6 coal. Energy Fuels 1988;2:719–20.
[7] Sakurovs R, Day S, Weir S. Relationships between the critical properties of gases and their high pressure sorption behavior on coals. Energy Fuels 2010;24:1781–7.
[8] Meyers RA. Coal structure. New York: Academic Press; 1982.
[9] Liu CJ, Wang GX, Sang SX, Rudolph V. Changes in pore structure of anthracite coal associated with CO_2 sequestration process. Fuel 2010;89:2665–72.
[10] Huxham IM, Rowatt B, Sherrington DC, Tetley L. Molecular architectural changes in hydrated macroporous styrene divinylbenzene resin sorbents revealed by transmission electron microscopy using image analysis. Polymer 1992;33:2768–77.
[11] Sinha S. Small-angle scattering from porous materials. In: Wong PZ, editor. Methods in the physics of porous media. San Diego, London: Academic Press; 1999. p. 223–62.
[12] Porod G. General theory. In: Glatter O, Kratky O, editors. Small-angle X-ray scattering. New York: Academic Press; 1982. p. 17–62.
[13] Radlinski AP, Boreham CJ, Lindner P, Randl O, Wignall GD, Hinde A, et al. Small angle neutron scattering signature of oil generation in artificially and naturally matured hydrocarbon source rock. Org Geochem 2000;31:1–14.
[14] Radlinski AP, Mastalerz M, Hinde AL, Hainbuchner M, Rauch H, Baron M, et al. Application of SAXS and SANS in evaluation of porosity, pore size distribution and surface area of coal. Int J Coal Geol 2004;59:245–71.
[15] Gethner JS. The determination of the void structure of macroporous coals by small-angle neutron scattering: void geometry and structure in Illinois No-6 bituminous coal. J Appl Phys 1986;59:1068–85.
[16] Hall PJ, Antxustegi M, Ruiz W. Contrast-matching small-angle neutron scattering evidence for the absence of a connected pore system in Pittsburgh No. 8 coal. Fuel 1998;77:1663–5.
[17] Antxustegi MM, Hall PJ, Calo J. Development of porosity in Pittsburgh No. 8 coal char as investigated by contrast-matching small-angle neutron scattering and gas adsorption techniques. Energy Fuels 1998;12:542–6.
[18] Hall PJ, Brown SD, Calo JM. The pore structure of the Argonne coals as interpreted from contrast matching small angle neutron scattering. Fuel 2000;79:1327–32.
[19] Mayama H, Tsujii K. Menger sponge-like fractal body created by a novel template method. J Chem Phys 2006;125(124706):1–10.
[20] Yamaguchi D, Mayama H, Koizumi S, Tsujii K, Hashimoto T. Investigation of self-assembled fractal porous-silica over a wide range of length scales using a combined small-angle scattering method. Eur Phys J 2008;B63:153–63.
[21] Melnichenko YB, Mayama H, Cheng G, Blach T. Monitoring phase behavior of sub- and super-critical CO_2 confined in porous fractal silica with 85% porosity. Langmuir 2010;26:6374–9.
[22] Ono Y, Mayama H, Furo I, Sagidullin AI, Masushima K, Ura H, et al. Characterization and structural investigation of fractal porous-silica over an extremely wide scale range of pore size. J Colloid Interf Sci 2009;336:215–25.
[23] Chathoth SM, Mamontov E, Melnichenko YB, Zamponi M. Diffusion and adsorption of methane confined in nano-porous carbon aerogel: a combined quasi-elastic and small-angle neutron scattering study. Microporous Mesoporous Mater 2010;132:148–53.
[24] <http://www.nist.gov/data/nist23.htm>.
[25] <http://neutrons.ornl.gov/hfir_instrument_systems/CG-2.shtml>.
[26] Barker JG, Glinka CJ, Moyer JJ, Kim MH, Drews AR, Agamalian M. Design and performance of a thermal-neutron double-crystal diffractometer for USANS at NIST. J Appl Cryst 2005;38:1004–11.
[27] Melnichenko YB, Radlinski AP, Mastalerz M, Cheng G, Rupp J. Characterization of the CO_2 fluid adsorption in coal as a function of pressure using neutron scattering techniques (SANS and USANS). Int J Coal Geol 2009;77:69–79.
[28] Radlinski AP, Busbridge TL, MacA Gray E, Blach TP, Cheng G, Melnichenko YB, et al. Dynamic micromapping of CO_2 sorption in coal. Langmuir 2009;25:2385–9.
[29] Sakurovs R, Radlinski AP, Melnichenko YB, Blach T, Cheng G, Lemmel H, et al. Stability of the bituminous coal microstructure upon exposure to high pressures of helium. Energy Fuels 2009;23:5022–6.
[30] Melnichenko YB, Wignall GD. Density and volume fraction of supercritical CO_2 in pores of native and oxidized aerogels. Int J Thermophys 2009;30:1578–90.
[31] Melnichenko YB, Wignall GD, Cole DR, Frielinghaus H. Adsorption of supercritical CO_2 in aerogels as studied by small-angle neutron scattering and neutron transmission techniques. J Chem Phys 2006;124(204711):1–11.
[32] In the control experiments, we did not observe any variation of $I(Q, P_{ZAC})$ with time up to ~12 hours.
[33] Fisher ME, DeGennes PG. Wall phenomena in a critical binary mixture. CR Acad Sci Ser B 1978;287:207–9.
[34] Higgins J, Benoit H. Polymers and neutron scattering. Oxford: Clarendon Press; 1994.
[35] Krivoglaz M. Theory of X-ray and thermal neutron scattering by real crystals. New York: Plenum Press; 1969.

Please cite this article in press as: Melnichenko YB et al. Accessibility of pores in coal to methane and carbon dioxide. Fuel (2011), doi:10.1016/j.fuel.2011.06.026